Crystal Chemistry and Luminescence of Ce^{3+}-Doped $Lu_2CaMg_2(Si,Ge)_3O_{12}$ and Its Use in LED Based Lighting

Anant A. Setlur,*,† William J. Heward,† Yan Gao,† Alok M. Srivastava,†
R. Gopi Chandran,‡ and Madras V. Shankar‡

GE Global Research, 1 Research Circle, Niskayuna, New York 12309, and GE Global Research, John F. Welch Technology Centre, Plot Number 122, EPIP-2, Hoodi Village, Whitefield Road, Bangalore, India 560 066

Received April 18, 2006. Revised Manuscript Received May 1, 2006

In this paper, we describe the formation and luminescence of a new garnet phosphor for light emitting diode (LED) based lighting, $Lu_2CaMg_2(Si,Ge)_3O_{12}:Ce^{3+}$. The regions for garnet phase formation are initially described with respect to larger rare earth substitution and show reasonable correlation to previous crystal chemistry studies for the garnet parent structure. While the pure silicate phosphor also has apatite second phases, a significant amount of Ce^{3+} enters the garnet phase, giving Ce^{3+} luminescence that is significantly redder when compared to typical Al^{3+} garnet phosphors with quantum efficiencies comparable to commercial Ce^{3+} garnet phosphors. Potential reasons for the emission red shift and the high quantum efficiency are discussed. Finally, the performance of these new phosphors is tested within LED based lamps. Lamps using these phosphors can reach color temperatures required for general illumination lighting and also have comparable phosphor conversion efficiencies when compared to lamps using typical garnet phosphors.

1. Introduction

Lamps based upon phosphor downconversion of blue light emitting diodes (LEDs) are potential replacements for conventional light sources such as incandescent or fluorescent lamps. Most of these lamps use $Y_3Al_5O_{12}:Ce^{3+}$ garnet (YAG:Ce) based phosphors dispersed in a polymer matrix and then coated on top of a blue LED.[1] The blue LED radiation is strongly absorbed by the allowed 4f → 5d transition of Ce^{3+}, leading to a yellow 5d → 4f (to the spin−orbit split $^2F_{7/2}$ and $^2F_{5/2}$ levels) emission band.[2] The combination of the yellow YAG:Ce emission and blue radiation bleeding through the phosphor coating gives white light. However, these lamps are inherently limited to color temperatures (CCTs) greater than 4500 K when the color point is restricted to be near the blackbody locus due to a lack of red spectral intensity. This prevents the use of these lamps in many general lighting applications, especially as replacements for lamps that have lower CCTs that make up the majority of the lighting market. Consequently, the development of red phosphors for LED lighting applications will be critical for market acceptance of these light sources in general illumination.

To meet the color requirements for general illumination lighting, new red phosphors have been invented and/or developed to improve the color of blue LED based lamps. These red phosphors are based on Eu^{2+}-doped hosts, such as (Ca,Sr)S:Eu^{2+} and $(Ba,Sr,Ca)_2Si_5N_8:Eu^{2+}$, where high crystal fields and covalency shift the position of the lowest $4f^65d$ levels of Eu^{2+} to very low energy.[3,4] The quantum efficiency (QE) of these phosphors can be >80%, and blends combining these phosphors with YAG:Ce give lamps with a wide range of CCTs (2800−5000 K) and good color rendering (CRI ∼ 70−90).[4,5]

In principle, one could also use Ce^{3+} as an activator for red phosphors since the position of the lowest 5d band is strongly influenced by host lattice selection and the intrinsic Ce^{3+} quantum efficiency can be high. However, at the current time, the only oxide Ce^{3+} phosphors that absorb blue radiation, emit in the yellow to red spectral regions, and have high quantum efficiencies are based on garnet host lattices. As discussed below, this appeared to be a limitation in the design of red Ce^{3+} phosphors for LED based lighting.

While the reasons for the very low energy position of the lowest Ce^{3+} 5d level in YAG are not completely clear, it is possible to alter the emission color of $\{Y\}_3[Al]_2(Al)_3O_{12}:Ce^{3+}$ phosphors via chemical substitutions into the $\{C\}_3[A]_2(D)_3O_{12}$ garnet structure,[6] where the {C} cations are eight-coordinated in dodecahedra, the [A] cations are octahedrally coordinated, and the (D) cations are tetrahedrally coordinated. For example, Gd^{3+} substitution on the {C} sites can shift the YAG:Ce^{3+} emission band by 15−20 nm.[7−9] In addition,

* To whom correspondence should be addressed. Phone: (518)387-6305. E-mail: setlur@research.ge.com.
† GE Global Research, Niskayuna.
‡ GE Global Research, Bangalore.

(1) Shimizu, Y.; Sakano, K.; Noguchi, Y.; Moriguchi, T. U.S. Patent 5,998,925, 1999.
(2) Blasse G.; Bril, A. *Appl. Phys. Lett.* **1967**, *11*, 53.
(3) Botty, G.; Hintzen, H. T.; van Krevel, J. W. H. U.S. Patent 6,682,663, 2004.
(4) Mueller, G. O.; Mueller-Mach, R. *Proc. SPIE* **2002**, *4776*, 122.
(5) Krames, M. M. presented at the DOE Solid State Lighting Workshop, Crystal City, VA, Nov 13−14, 2003 (unpublished).
(6) Geller, S. *Z. Kristallogr.* **1967**, *125*, 1.
(7) Tien, T. Y.; Gibbons, E. F.; DeLosh, R. G.; Zacmanidis, P. J.; Smith, D. E.; Stadler, H. L. *J. Electrochem. Soc.* **1973**, *120*, 278.
(8) Holloway, W. W.; Kestigian, M. *J. Opt. Soc. Am.* **1969**, *59*, 60.

10.1021/cm060898c CCC: $33.50
Published on Web 06/07/2006

Gd^{3+} substitution on the {C} sites and $Mg^{2+}-Si^{4+}$ substitution on the [A] and (D) sites, respectively, lead to Ce^{3+} emission maxima at ~615 nm.[9] However, further emission red shifts are limited by garnet phase instability and lower efficiencies at room and/or elevated temperatures.[9] However, these compositions give an initial design rule for red Ce^{3+} emission in garnet hosts. The $Mg^{2+}-Si^{4+}$ couple on the [A] and (D) sites can shift the Ce^{3+} emission band to low energies. This is apparently due to a stronger crystal field splitting for the Ce^{3+} 5d levels induced by the replacement of $[Al^{3+}]-(Al^{3+})$ with $[Mg^{2+}]-(Si^{4+})$. However, there have been no further reports that correlate the luminescence of $Mg^{2+}-Si^{4+}$-doped YAG with the crystallography of these substitutions. Therefore, the findings of Robertson et al.[9] are taken as phenomenological design rules for Ce^{3+} luminescence in garnets. We note that strong crystal fields are observed in many silicates, especially in comparison to borate and phosphate hosts.[10]

These phenomenological design rules for red Ce^{3+} emission in garnets do not guarantee the discovery of useful materials, since new compositions need to be designed that have both red emission and high quantum efficiencies at room and elevated temperatures. However, taking the design rules for emission color based upon $Mg^{2+}-Si^{4+}$ substitution in garnets is generally limited due to garnet phase stability issues when smaller cations, such as Al^{3+} ($r^{IV} = 0.53$ Å [11]) or Si^{4+} ($r^{IV} = 0.40$ Å [11]), occupy the tetrahedral (D) sites.[6] For example, while Ga^{3+} ($r^{IV} = 0.61$ Å [11]) garnets form for most of the lanthanides ($Pr^{3+}-Lu^{3+}$), $REAlO_3$ perovskites are more stable than $RE_3Al_5O_{12}$ garnets for lanthanides larger than Tb^{3+}.[6] Silicate garnet synthesis by conventional solid-state reactions are even more limited; there have been very few silicate garnet compositions, such as $Ca_3Cr_2Si_3O_{12}$ [12] or $Ca_3Sc_2Si_3O_{12}$ [13] made at ambient pressures. Other methods such as sol−gel,[14] glass devitrification,[15] and lithium molybdate fluxing[16] have been used to make $Ca_3[Cr,Al]_2Si_3O_{12}$, $Mn_3Al_2Si_3O_{12}$, and $Ca_3Fe_2Si_3O_{12}$, respectively. Reports of silicate garnets with trivalent ions in the {C} site are even more limited with a single report of hydrothermal garnet synthesis in the $RE_2O_3-(Mg,Ni)O-SiO_2$ [17] system, where RE = Y^{3+}, Lu^{3+}, Yb^{3+}, or Ho^{3+}. There also have been reports in the patent literature regarding RE^{3+} or Y^{3+} substitution into the [A] sites of $Ca_3Sc_2Si_3O_{12}$,[13] leading to Ce^{3+}-doped phosphors with emission maxima similar to typical Al^{3+} garnet phosphors. In these phosphors, we believe that there is some occupation of the dodecahedral {C} sites by RE^{3+} or Y^{3+}, so these results show that ambient pressure synthesis of silicate garnets with some degree of RE^{3+} substitution is possible. However, the reported Ce^{3+} emission spectra do not satisfy the red phosphor requirements for LED lighting applications, so new materials are still needed. In general, garnet formation in systems with RE_2O_3 and SiO_2 at ambient pressure is strongly limited by the competitive formation of apatites (e.g., $RE_{9.33}(SiO_4)_6O_2$ [18]) or other oxysilicate phases (e.g., RE_2SiO_5 or $RE_2Si_2O_7$) that do not efficiently absorb blue LED radiation.

Consequently, while the work of Robertson et al.[9] gives phenomenological crystal chemistry rules for red Ce^{3+} emission in garnet phosphors, garnet phase stability issues made it seem unlikely for implementation into an efficient Ce^{3+} red phosphor for blue LED systems. Furthermore, since there are currently no non-garnet Ce^{3+} based oxide phosphors that absorb blue radiation and have efficient yellow-orange luminescence, it also seemed unlikely that Ce^{3+} based oxide phosphors can meet the requirements for a red LED phosphor.

However, in this paper, we describe the synthesis and luminescent properties of a new silicate garnet phosphor, $Lu_2CaMg_2(Si,Ge)_3O_{12}:Ce^{3+}$, that can meet the requirements for red LED phosphors. While some of these phosphor samples are not X-ray single phase garnets, the relative amounts of second phases such as apatites or RE oxysilicates do not significantly interfere with the efficient garnet luminescence. The composition regions for phase stability, and the effect of composition on Ce^{3+} luminescence in these materials will also be discussed. Unlike other garnets with red Ce^{3+} emission,[9] the quantum efficiency of these phosphors is comparable to current garnet phosphors, making them practical for use in typical LED packages. The luminescent properties of these new garnets are explained through structural and composition comparison with YAG:Ce phosphors, giving potential reasons for the red emission color, high quantum efficiency, and low thermal quenching for these new materials. Finally, initial testing of these phosphors under blue LED excitation will also be described.

2. Experimental Methods

Powder phosphor samples were made using mixtures of high-purity RE_2O_3, CeO_2, $CaCO_3$, MgO, silicic acid, and GeO_2 and fired under reducing conditions at 1300−1450 °C for 5−10 h. All samples are doped with 4−6 at. % (nominal) Ce^{3+}, replacing other RE^{3+} ions, unless specifically mentioned otherwise. This doping is implied whenever any compositions are described in this paper. In addition, the compositions that are quoted in this paper are quoted as the nominal compositions. Samples are then ground to a median particle size of ~10 μm as measured by light scattering methods (Horiba LA-910).

Powder X-ray diffraction (XRD) data were collected on either a $\theta-2\theta$ Bruker D8 Advance diffractometer using a Ni-filter, a NaI(Tl) scintillation detector with 1 mm antiscatter slits, and a 0.1 mm detector slit or a $\theta-\theta$ Bruker D8 Advance diffractometer equipped with a linear position-sensitive detector (PSD-50m, M. Braun) with an aperture slit of 0.6 mm. Step scans were performed from 15 to 90° 2θ and a step size of 0.02° with a count time of 2 s/step. NIST-certified SRM 640c silicon was used as an external calibration standard. Generally, refined lattice parameters of XRD patterns

(9) Robertson, J. M.; van Tol; M. W.; Smits, W. H.; Heynen, J. P. H. *Philips J. Res.* **1981**, *36*, 15.
(10) Dorenbos, P. *Phys. Rev. B* **2001**, *64*, 125117.
(11) Shannon, R. D.; Prewitt, C. T. *Acta Crystallogr., Sect. B: Struct. Crystallogr. Cryst. Chem.* **1969**, *25*, 925. Shannon, R. D.; Prewitt, C. T. *Acta Crystallogr., Sect. B: Struct. Crystallogr. Cryst. Chem.* **1970**, *26*, 1046.
(12) Geller, S.; Miller, C. E. *Am. Mineral.* **1959**, *44*, 445.
(13) Shimomura, Y.; Kijima, N. U.S. Pat. Appl. 2004/0251809A1, 2004.
(14) Carda, J.; Monros, G.; Esteve, V.; Amigo, J. M. *J. Solid State Chem.* **1994**, *108*, 24.
(15) Yoder, H. S.; Keith, M. L. *Am. Mineral.* **1951**, *36*, 519.
(16) Geller, S.; Williams, H. J.; Espinosa, G. P.; Sherwood, R. C. *Bell Syst. Tech. J.* **1964**, *48*, 565.
(17) Ito, J. *Mater. Res. Bull.* **1967**, *2*, 1093.
(18) Felsche, J. *J. Solid State Chem.* **1972**, *5*, 266.

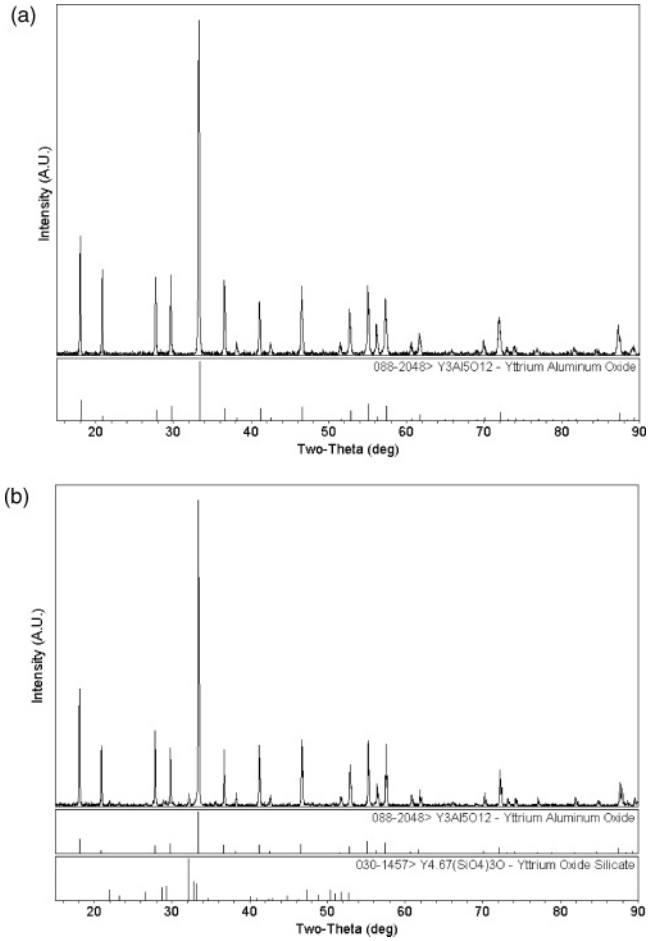

Figure 1. Powder X-ray diffraction spectra for nominal compositions of (a) $(Lu_{0.955}Ce_{0.045})_2CaMg_2Si_{2.2}Ge_{0.8}O_{12}$ and (b) $(Lu_{0.955}Ce_{0.045})_2CaMg_2Si_3O_{12}$.

taken on in-house instruments had least-squares errors of ~0.0005 Å. Occasionally, numerous patterns of the same sample in this study were collected and refined, and the standard deviation of the resulting lattice parameters was determined. The largest error using this methodology approached 0.001 Å. Though in most cases the error was less, we adopted an error of 0.001 Å for the lattice parameter, which proved satisfactory given the large differences in the various garnets in this paper.

A synchrotron X-ray diffraction pattern was measured on a powder sample with a nominal composition of $Lu_{1.999}Ce_{0.001}CaMg_2Si_3O_{12}$. The sample was ground and loaded into a 0.5 mm quartz capillary and was measured at the X7B beamline, NSLS, Brookhaven National Laboratory, with a wavelength of 0.922 Å. The sample was oscillated 60° in ϕ during measurement to probe a larger number of grains. The data were taken with a Mar345 image plate system and integrated by using the program Fit2D[19] in a 20 °C cake along the vertical direction, along which synchrotron X-rays are nearly linearly polarized (polarization factor ~ 0.97). The structure refinement was performed using the GSAS (General Structure Analysis System) software package.[20] The garnet phase was refined by the Rietveld method while the apatite phase was refined by the LeBail method[21] that does not use the atomic parameters of the apatite phase. In this manner, the apatite impurity peaks can be fitted without knowing its exact composition, and the Rietveld refinement can focus on the garnet phase that is the focus of this work. Capillary absorption was applied in this refinement. After convergence of the refinement, the inspection of the fit between observed and calculated patterns showed that the contribution of the apatite phase to the total intensity is much less than that from the garnet phase. There were only a few cases where apatite peaks overlapped with garnet peaks. Therefore, using the LeBail method on the apatite phase does not appear to skew the results on the Rietveld refinement of the garnet phase.

Phosphor emission and excitation were made using powders pressed into an aluminum plaque on a SPEX Fluorolog spectrofluorometer with corrections for Xe lamp intensity and instrument response. All measurements are taken at room temperature unless otherwise mentioned. Relative quantum efficiency measurements used commercial Ce-doped garnet phosphors as standards. Diffuse reflectance measurements used the same spectrometer with $BaSO_4$ powder used as a reflectance standard. High-temperature luminescence measurements used powders pressed into a phosphor plaque with resistive heaters and a thermocouple that are attached to a standard temperature controller. Time-resolved measurements were made at room temperature using a PicoQuant laser at 394 nm coupled into an Edinburgh F900 spectrofluorometer with a R928-P Hamamatsu photomultiplier tube detector. The full width at half-maximum (fwhm) of the laser pulse convoluted with the overall system response is <3 ns. Initial testing of lower CCT phosphor blends using $Lu_2CaMg_2Si_3O_{12}:Ce^{3+}$ and typical Ce^{3+}-doped garnet phosphors used a light source with six blue (λ_{max} ~ 466 nm) LEDs with a phosphor/silicone suspension coated onto a glass or clear plastic sheet.

3. Results and Discussion

3.1. Silicate Garnet Phase Formation. As mentioned above, there have been limited reports on the ambient pressure synthesis of silicate garnets. However, garnets with larger Ge^{4+} ions on the tetrahedral (D) sites can be made at ambient pressure with a wide range of cations on the {C} and [A] sites. Among these garnets, Reinen has described a variety of RE^{3+} or Y^{3+} garnets with the general composition $\{RE_2Ca\}[Mg]_2(Ge)_3O_{12}$.[22] When these garnet compositions are doped with Ce^{3+}, the body color of these powders is yellow-orange, indicating that Ce^{3+} has been incorporated into these garnets. However, there is little to no Ce^{3+} luminescence at room temperature. The low luminescence efficiency is most likely due to Ce^{3+} photoionization[23] due to the relatively small band gap of germanate hosts. For example, strong Ce^{3+} luminescence quenching has also been observed in other germanate garnets, such as $Ca_3Sc_2Ge_3O_{12}$.[24] This quenching process can be thought of as a metal−metal charge transfer between Ce^{3+} and Ge^{4+}, a d^{10} ion. Replacing d^{10} ions with ions that have noble gas configurations in garnets can significantly improve Ce^{3+} efficiency as in the $Y_3Al_5O_{12}-Y_3Ga_5O_{12}$ system.[2,7−9] Therefore, one potential method to improve the Ce^{3+} luminescence efficiency would be to replace Ge^{4+} with Si^{4+}.

Initially, compositions with Lu^{3+} were investigated because garnet phase stability typically increases with smaller tri-

(19) Hammersley, A. P. ESRF Internal Report, ESRF97HA02T, 1997.
(20) Larson, A. C.; Von Dreele, R. B. Report LAUR 86-748, Los Alamos National Laboratory, Los Alamos, NM, 2000.
(21) LeBail, A.; Duroy, H.; Fourquet, J. L. *Mater. Res. Bull.* **1988**, *23*, 447
(22) Reinen, D. *Z. Anorg. Allg. Chem.* **1964**, *327*, 238.
(23) Blasse, G.; Schipper, W.; Hamelink, J. J. *Inorg. Chim. Acta* **1991**, *189*, 77.
(24) Pinelli, S.; Bigotta, S.; Toncelli, A.; Tonelli, M.; Cavalli, E.; Bovero, E. *Opt. Mater.* **2004**, *25*, 91.

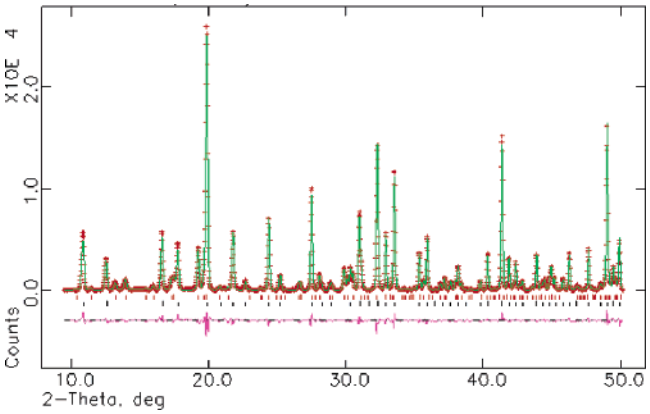

Figure 2. Synchrotron powder X-ray diffraction spectra of $(Lu_{0.999}Ce_{0.001})_2CaMg_2Si_3O_{12}$ (nominal composition) with simulated spectra (crosses) from Rietveld refinement of garnet phase and LeBail refinement of apatite phase. The difference between the calculated and simulated spectra is plotted on the lower curve in the figure.

Table 1. Crystallographic and Spectroscopic Properties (λ_{ex} = 470 nm) for $(Lu_{0.955}Ce_{0.045})_2CaMg_2Si_{3-x}Ge_xO_{12}$

x	a_0 (Å)	rel QE	I(100 °C)/I(RT) (% basis)
0	11.975	100	85
0.6	11.99	78	73
0.8	12.025	78	67
1.0	12.055	67	57

Table 2. Refined Structural Parameters and Selected Bond Lengths for $Lu_{1.999}CaMg_2Si_3O_{12}$ (Nominal Composition)[a]

atom	Wyckoff	x	y	z	occupancy	U_{iso}
Mg	16a	0	0	0	1.00	0.012(2)
Ca	24c	0.125	0	0.25	0.40(1)	0.0080(5)
Lu	24c	0.125	0	0.25	0.60(1)	0.0080(5)
Si	24d	0.375	0	0.25	1.00	0.010(2)
O	96h	0.0351(6)	0.0538(6)	0.6578(5)	1.00	0.023(3)

[a] Space group: *Ia*3*d* (No. 230); a_0 = 11.9758(3); R_p = 7.54% and $R(F^2)$ = 3.18% for 63 garnet reflections. Selected bond lengths: {Lu,Ca}−O, 2.315 Å; {Lu,Ca}−O, 2.418 Å; [Mg]−O, 2.040 Å; (Si)−O, 1.672 Å.

valent {C} cations.[6] As more Si^{4+} is substituted into the $\{Lu_2Ca\}[Mg]_2(Si_xGe_{3-x})O_{12}$ composition, secondary phases such as apatites or other RE^{3+} oxysilicates begin to form when $x > 2.4$ (Figure 1). For the nominal composition $\{Lu_2Ca\}[Mg]_2(Si)_3O_{12}$, *a pure silicate*, garnet is the majority phase with primarily apatite as the main second phase. Other oxysilicate phases such as Lu_2SiO_5 or $Lu_2Si_2O_7$ are also occasionally observed as secondary phases. The lattice parameter of these garnets (Table 1) show a clear decrease in cell dimension with higher Si^{4+} concentrations, as expected given the smaller ionic radii of Si^{4+} vs Ge^{4+}. However, the lattice parameter does not follow a clear linear relationship with Si^{4+} concentration as expected by Vegard's Law: the $\{Lu_2Ca\}[Mg]_2(Si)_3O_{12}$ composition has a larger lattice parameter than expected. The Rietveld refinement of the pure silicate sample (Figure 2 and Table 2) shows that Lu^{3+} and Ca^{2+} are randomly distributed on the dodecahedral {C} sites. However, the electron density at the dodecahedral {C} site is slightly less than expected from the nominal composition of $\{Lu_2Ca\}[Mg]_2(Si)_3O_{12}$. This is thought to be due to a deviation from the nominal Lu:Ca ratio of 2:1 (Table 2). This deviation from nominal stoichiometry could be balanced by oxygen vacancies, but the differences in oxygen occupancy are too small to be determined in these powder XRD experiments. Oxygen vacancies have been measured and observed in garnets through electrical and ionic conductivity measurements,[25] but it is not known if such a high concentration of oxygen vacancies as indicated from the Rietveld refinement can be supported in the silicate garnet. The deviation from the stoichiometric Lu:Ca ratio to lower values in the pure silicate garnet could also explain the deviation from Vegard's Law since the ionic radii of Ca^{2+} is larger than Lu^{3+}. Further investigation and structural characterization of the entire solid solution series and the pure silicate garnet is necessary to clarify this issue. We also note that deviations from Vegard's Law have been measured in silicate and aluminate garnets with compositions that are close to regions of phase instability,[26,27] similar to the conditions in this system as discussed below.

The dodecahedral and octahedral bond lengths calculated from the Rietveld analysis of the pure silicate garnet are in reasonable agreement with the bond lengths in other garnets[26,27] (Table 2). The {Lu,Ca}−O bond lengths are slightly longer compared to those in $Lu_3Al_5O_{12}$,[26] as expected given the presence of larger Ca^{2+} ions on the dodecahedral sites. Similarly, the [Mg]−O bond lengths are comparable to other garnets with larger ions (i.e., Sc^{3+}, Ga^{3+}) occupying the octahedral sites.[6,26] However, the (Si)−O bond length of 1.672 Å is somewhat longer compared to the (Si)−O bond lengths in hydrothermally grown or natural garnets, where the (Si)−O bond lengths are typically between 1.63 and 1.65 Å.[27] Presumably, the combination of larger ions on the dodecahedral and octahedral sites causes a longer (Si)−O bond length. The Rietveld refinement also shows that the bond strain for the octahedral and tetrahedral sites, determined by the difference in bond angle for ideal octahedra and tetrahedra (92.4° and 87.6° vs 90° for octahedra and 100.05° and 114.38° vs 109.47°), is not unusual for aluminate[26] or silicate[27] garnets. The dodecahedral bond angles are also similar to other silicate garnets. However, the O−{C}−O bond angle for the dodecahedral−tetrahedral shared edge is significantly smaller in this silicate garnet (67.54°) in comparison to typical aluminate garnets (71.66° for $Y_3Al_5O_{12}$ [26]). This is not surprising considering that the anion−anion repulsion for the dodecahedral−tetrahedral shared edge should be reduced in the silicate garnets due to the higher charge and smaller size of Si^{4+} vs Al^{3+}.[27]

While the bond angles for this silicate garnet are not unusual, the (Si)−O bond length is longer compared to typical silicates. Consequently, any further expansion of the host lattice should destabilize garnet formation. This is supported by the observation that larger trivalent ions, such as Y^{3+}, Gd^{3+}, or Tb^{3+}, do not form $RE_2CaMg_2Si_3O_{12}$ (nominal) garnets at ambient pressure. In addition, replacing ~20% of the Lu^{3+} with Y^{3+} and Tb^{3+} (Figure 3a) results in an increase in the amount of apatite second phases, although quantifying this difference is beyond the scope of this report. Even smaller (<10%) Gd^{3+} additions (with Ce^{3+} doping) almost completely destabilize garnet formation (Figure 3b) under similar synthesis conditions. As noted above, larger

(25) Rotman, S. R.; Tandon, R. P.; Tuller, H. L. *J. Appl. Phys.* **1985**, *57*, 1951.
(26) Euler, F.; Bruce, J. A. *Acta Crystallogr.* **1965**, *19*, 971.
(27) Novak, G. A.; Gibbs, G. V. *Am. Mineral.* **1971**, *56*, 791.

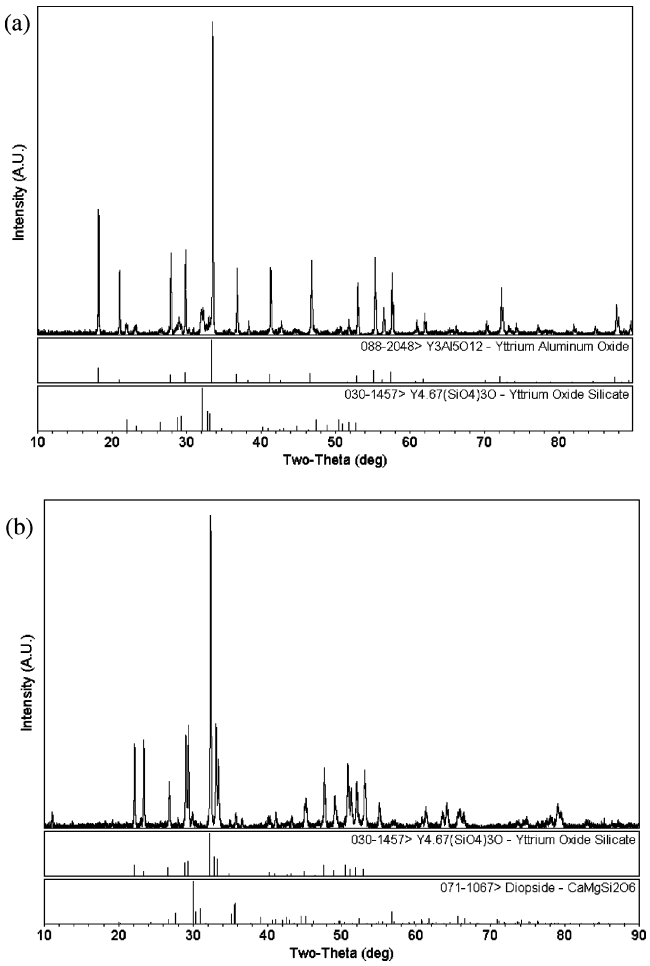

Figure 3. Powder X-ray diffraction spectra for nominal compositions of (a) $(Lu_{0.785}Ce_{0.04}Tb_{0.155})_2CaMg_2Si_3O_{12}$ and (b) $(Lu_{0.875}Ce_{0.04}Gd_{0.085})_2CaMg_2Si_3O_{12}$.

cations on the {C} site generally destabilize the garnet structure, so it is not surprising that the solubility of larger ions on the {C} site in $\{Lu_2Ca\}[Mg]_2(Si)_3O_{12}$ is limited under ambient pressure synthesis conditions. Preliminary results indicate that replacing Si^{4+} with Ge^{4+} enhances the substitution of larger ions on the dodecahedral {C} sites, but this was not extensively studied.

3.2. Ce^{3+} Luminescence in the Silicate Garnets. As expected for a garnet host, the lowest Ce^{3+} $4f^1 \rightarrow 5d^1$ absorption transition for $\{Lu_2Ca\}[Mg]_2(Si)_3O_{12}$ is in the blue spectral region (Figure 4a), leading to a yellow-orange body color. The position of the lowest Ce^{3+} $4f^1 \rightarrow 5d^1$ absorption transition is at lower energy in $\{Lu_2Ca\}[Mg]_2(Si)_3O_{12}$ versus YAG, implying a stronger crystal field on Ce^{3+} in this host lattice, following previous reports that garnets with $[Mg^{2+}]-(Si^{4+})$ substitution have stronger crystal fields.[11] Excitation into this absorption band at 470 nm gives a luminescence band with a maxima of ~605 nm (Figure 4b), an emission red shift of ~1700 cm^{-1} compared to YAG:Ce^{3+}. The emission spectra for samples with 4−6 at. % Ce (nominal) are generally constant for excitation wavelengths from 420 to 500 nm. However, at much lower Ce^{3+} concentrations (0.1% nominal), excitation at short wavelengths leads to a yellow emission band, while excitation at longer wavelengths leads to a red-orange emission band (Figure 5a). Correspondingly, excitation spectra for longer wavelengths are also

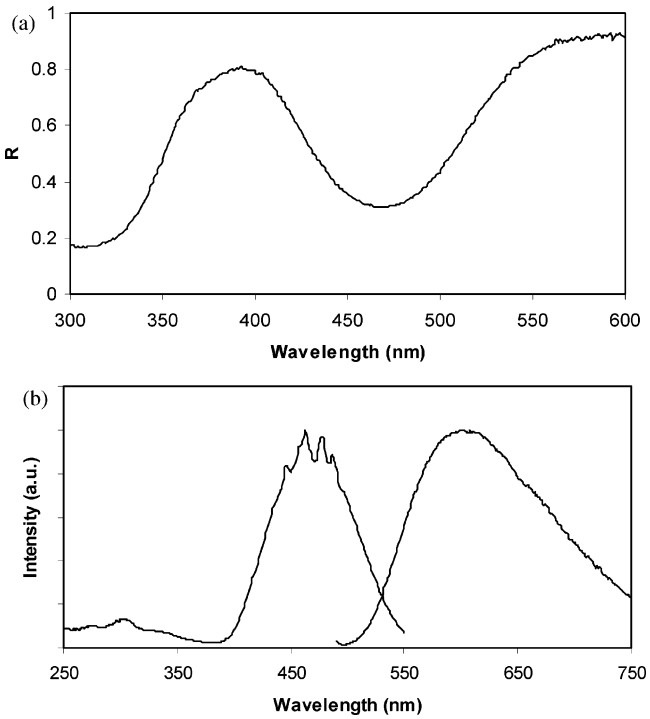

Figure 4. (a) Diffuse reflectance spectra of $(Lu_{0.94}Ce_{0.06})_2CaMg_2Si_3O_{12}$ showing a strong absorption in the blue spectral region indicative of a Ce^{3+} $4f^1 \rightarrow 5d^1$ absorption in garnets. (b) Emission ($\lambda_{ex} = 470$ nm) and excitation ($\lambda_{em} = 605$ nm) spectra for $(Lu_{0.94}Ce_{0.06})_2CaMg_2Si_3O_{12}$. The sharp lines in the excitation spectra are experimental artifacts from the Xe lamp source.

shifted to lower energy (Figure 5b). Among the phases present in these samples, only the garnet phase should have Ce^{3+} absorption/excitation bands in the blue spectral region and emission bands in the yellow/orange; Ce^{3+}-doped silicate apatites should not have any absorption in the visible.[28] In addition, the Rietveld refinement of the silicate garnet shows no evidence for multiple garnet phases. Therefore, the emission bands in these samples are thought to be due to different Ce^{3+} sites in the garnet arising from the dodecahedral site disorder between Lu^{3+} and Ca^{2+} in $\{Lu_2Ca\}[Mg]_2(Si)_3O_{12}$.

Since there is significant spectral overlap between the emission of the high-energy sites and the excitation of the low-energy sites (Figure 5), energy transfer should occur between the high- and low-energy Ce^{3+} ions. The critical concentration, x_c, to quench the high-energy emission through dipole−dipole interactions can be estimated by[29−31]

$$R_c^6 = (6.6 \times 10^{27})(4.8 \times 10^{-16})E^{-4} f\,\mathrm{SO} \qquad (1)$$

$$x_c = \frac{6V}{\pi N R_c^3} \qquad (2)$$

where R_c is the critical distance for energy transfer, f is the oscillator strength of the Ce^{3+} transitions (~0.01), SO is the spectral overlap of the high-energy ($5d \rightarrow {}^2F_{5/2}$) Ce^{3+} emission and the low-energy Ce^{3+} excitation (~0.275 eV^{-1}), E is the energy of maximum overlap (2.35 eV), V is the unit

(28) de Vries, A. J.; Blasse, G. *Mater. Res. Bull.* **1986**, *21*, 683.
(29) Dexter, D. L. *J. Chem. Phys.* **1953**, *21*, 836.
(30) van Schaik, W.; Lizzo, S.; Smit, W.; Blasse, G. *J. Electrochem. Soc.* **1993**, *140*, 216.
(31) Blasse, G. *Philips Res. Rep.* **1969**, *24*, 131.

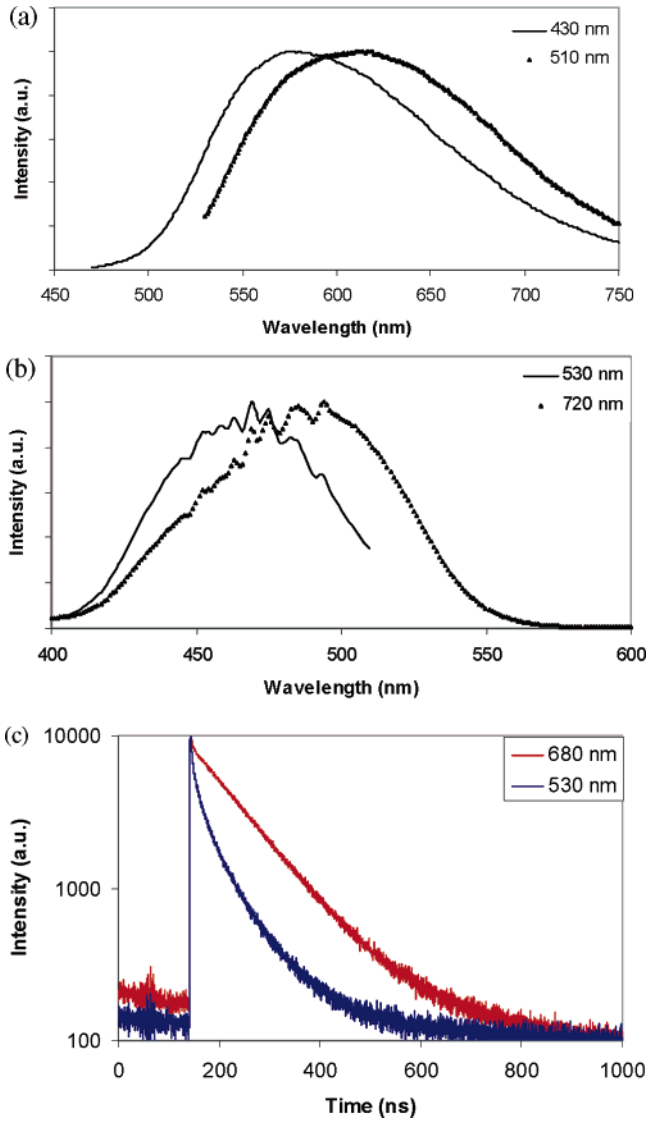

Figure 5. (a) Emission spectra for high-energy (λ_{ex} = 430 nm) and low-energy (λ_{ex} = 510 nm) excitation of $(Lu_{0.999}Ce_{0.001})_2CaMg_2Si_3O_{12}$. (b) Excitation spectra for high-energy (λ_{em} = 530 nm) and low-energy (λ_{ex} = 720 nm) emission of $(Lu_{0.999}Ce_{0.001})_2CaMg_2Si_3O_{12}$. (c) Decay profiles for $(Lu_{0.94}Ce_{0.06})_2CaMg_2Si_3O_{12}$ at different wavelengths to probe the various Ce^{3+} "sites" within this material.

cell volume, and N is the number of ions in a unit cell. The excitation spectrum for the low-energy Ce^{3+} sites is estimated by fitting the excitation curve for λ_{em} = 720 nm (Figure 5b) to two Gaussians and using the lower energy Gaussian curve. In these calculations, donor energy migration is not taken into account, so the calculated value of x_c should be considered as an overestimate. Using eqs 1 and 2, R_c is calculated to be ~26 Å, with $x_c \sim 0.008$. Clearly, at low Ce^{3+} concentrations, the luminescence from the high-energy Ce^{3+} ions will be somewhat quenched and these ions will sensitize the lower energy Ce^{3+} ions. The samples with 4.5% Ce^{3+} (nominal) have emission spectra under 470 nm excitation (Figure 4b) that are significantly broader than either the low-energy or high-energy Ce^{3+} emission for samples with 0.1% Ce^{3+} (nominal), a strong indication of energy transfer between the high- and low-energy Ce^{3+} sites. This is also supported by the strongly nonexponential decay profile of the high-energy site (λ_{em} = 530 nm), compared to the

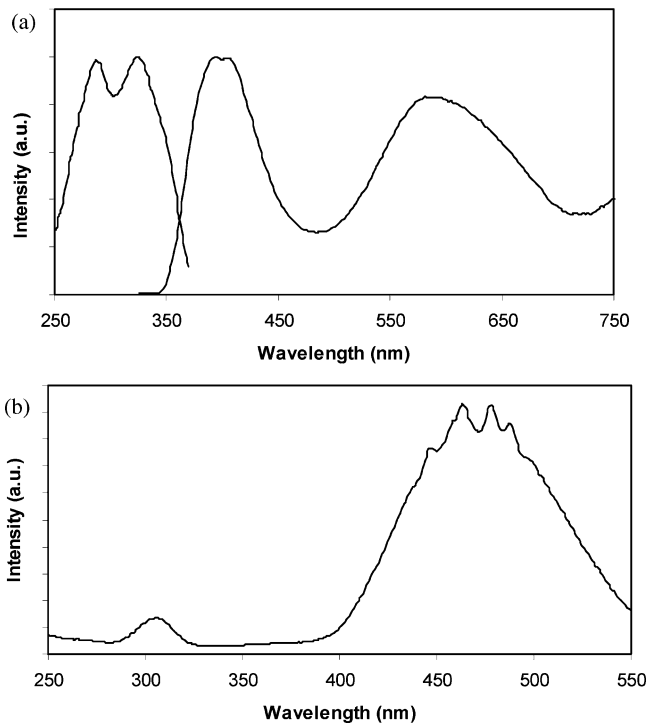

Figure 6. (a) Emission spectra for excitation into the broad UV absorption band of $(Lu_{0.94}Ce_{0.06})_2CaMg_2Si_3O_{12}$ samples (λ_{ex} = 320 nm) and excitation spectra for UV emission band of $(Lu_{0.94}Ce_{0.06})_2CaMg_2Si_3O_{12}$ samples (λ_{ex} = 395 nm). (b) Excitation spectra (λ_{em} = 600 nm) measured at 200 °C for $(Lu_{0.94}Ce_{0.06})_2CaMg_2Si_3O_{12}$.

exponential decay profile ($\tau \sim 100$ ns) for the low-energy site (λ_{em} = 680 nm) (Figure 5c).

The Lu^{3+}/Ca^{2+} disorder combined with energy transfer between Ce^{3+} ions also means that the caution must be taken in any quantitative analysis of the spin−orbit splitting between the $^2F_{7/2}$ and $^2F_{5/2}$ $4f^1$ levels and the Ce^{3+} Stokes shift. Therefore, we focus on only the low-energy Ce^{3+} site (λ_{ex} = 530 nm), since energy-transfer effects will be minimized for this site. The spin−orbit splitting between the $^2F_{7/2}$ and $^2F_{5/2}$ levels is estimated at ~1900 cm^{-1} using a Gaussian least-squares fit to the low-energy emission bands, a reasonable value for this splitting. The Stokes shift of the low-energy band is estimated at 2550 cm^{-1}, which is comparable to our measured value of ~2700 cm^{-1} in YAG:Ce.

Unlike the clearly resolved 4f → 5d absorption transition in the blue spectral region, the diffuse reflectance (Figure 4a) and excitation (Figure 4b) bands in the deeper UV cannot be easily assigned, unlike the UV excitation bands in YAG:Ce^{3+}.[32] Excitation of $\{Lu_2Ca\}[Mg]_2(Si)_3O_{12}$ samples in the deeper UV absorption band (λ_{ex} = 320 nm) gives a deep blue emission band as well as the orange-red garnet emission band (Figure 6a). The excitation and emission for this deep blue emission band correlates reasonably well with previous reports on the luminescence of Ce^{3+}-doped silicate apatites[28] and/or oxysilicates such as Lu_2SiO_5[33] that are present as secondary phases in these samples. The deep blue emission from the impurity phases can be absorbed by the garnet in

(32) Robbins, D. J. *J. Electrochem. Soc.* **1979**, *126*, 1550.
(33) Suzuki, H.; Tombrello, T. A.; Melcher, C. L.; Schweitzer, J. S. *IEEE Trans. Nucl. Sci.* **1993**, *40*, 380.

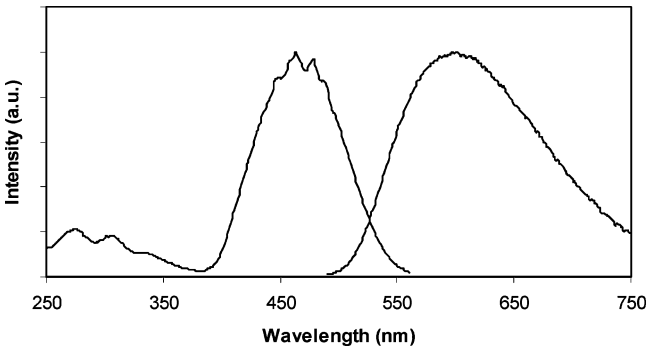

Figure 7. Room-temperature excitation (λ_{em} = 600 nm) and emission spectra (λ_{ex} = 470 nm) of $(Lu_{0.94}Ce_{0.06})_2CaMg_2Si_{2.2}Ge_{0.8}O_{12}$.

these samples, leading to garnet luminescence and spurious UV peaks in the garnet excitation spectra. The relative intensity of the broad UV diffuse reflectance band compared to the garnet diffuse reflectance band (Figure 4a) in the blue also indicates that the larger Ce^{3+} ion (r^{VIII} = 1.28 Å [11]) has reduced solubility in the garnet under these synthesis conditions, in accordance with the trends for phase stability reported above. Analysis of the Ce^{3+} 5d crystal field splitting is difficult at room temperature since the secondary phase absorption/excitation bands obscure the higher energy Ce^{3+} 5d levels in $\{Lu_2Ca\}[Mg]_2(Si)_3O_{12}$. However, at high temperatures (150−200 °C), the excitation spectra in the UV sharpen into a single band at ∼305 nm (Figure 6b). This band is assigned to a higher energy Ce^{3+} $4f^1 \rightarrow 5d^1$ garnet absorption band since Ce^{3+} luminescence in many of the secondary phases is strongly quenched at these temperatures.[34] This is supported by excitation spectra of a sample of $Lu_2CaMg_2Si_3O_{12}$:Ce^{3+} that was made via hydrothermal synthesis that has reduced second phase formation and has only a single excitation band at ∼305 nm. Unlike the blue excitation band, the position of the UV excitation band does not significantly change for the low-energy or high-energy Ce^{3+} sites that arise from {C} site disorder. Consequently, the splitting between the lowest two Ce^{3+} 5d levels in $\{Lu_2Ca\}[Mg]_2(Si)_3O_{12}$ ranges from ∼11 000−12 000 cm^{-1} vs ∼7700 cm^{-1} in YAG.

Compositions with Ge^{4+} have the lowest energy Ce^{3+} excitation and emission bands shifted to higher energies (Figure 7), implying a smaller crystal field with the substitution of larger cations on the tetrahedral (D) site. The splitting of the two lowest Ce^{3+} 5d levels is somewhat smaller compared to the pure silicate garnets (Figure 7). Similar trends for Ce^{3+} luminescence have been observed when replacing Al^{3+} with Ga^{3+} in typical Al^{3+} garnets.[7−9] However, in the Si^{4+}/Ge^{4+} garnets, the position of the high-energy excitation band is relatively constant, while the lower energy band moves to higher energy. Even with the blue shift in the lowest 5d bands with Ge^{4+} substitution, the splitting of the two lowest Ce^{3+} bands in these Si^{4+}/Ge^{4+} based garnets is still much larger (>2500 cm^{-1}) when compared to typical Al^{3+}/Ga^{3+} garnets.

The position of the lowest 5d level for lanthanide ions in inorganic hosts is dependent upon two separate factors: the shift in the 5d centroid from the free ion levels and the crystal field splitting of the 5d manifold.[10] The 5d centroid shift, ϵ_c, in $\{Lu_2Ca\}[Mg]_2(Si)_3O_{12}$ can be estimated by taking into account an average cation electronegativity combined with the {Lu,Ca}−O bond lengths from the Rietveld refinement:[10,35,36]

Table 3. Spectroscopic Properties for the Ce^{3+} 5d Manifold in the Garnets

composition	centroid shift (cm^{-1}) (estd)	10Dq (cm^{-1}) (estd)	splitting of lowest E_g levels (cm^{-1})
$Lu_3Al_5O_{12}$	14 300	18 400	6600
$Y_3Al_5O_{12}$	14 250	18 450	7600
$Lu_2CaMg_2Si_3O_{12}$	13 300	18 000−18 500	11 000−12 000

$$\epsilon_c = 1.79 \times 10^{13} \sum_{i=1}^{N} \frac{\alpha_{sp}^{\ i}}{(R_i - 0.6\Delta R)^6} \quad (3)$$

$$\alpha_{sp} = 0.33 + \frac{4.8}{\chi_{av}^{\ 2}} \quad (4)$$

where R_i is the Ce^{3+}-anion distance, N represents the number of anions coordinated to Ce^{3+}, ΔR is the difference in ionic radii for Lu^{3+}/Ca^{2+} and Ce^{3+}, and χ_{av} is the weighted average of the cation electronegativity in a given oxide host lattice. The estimated 5d centroid shift is ∼13 300 cm^{-1}, or ∼1000 cm^{-1} *smaller* compared to typical Al^{3+} garnets (Table 3), meaning that while the lowest 5d level is at lower energy in $\{Lu_2Ca\}[Mg]_2(Si)_3O_{12}$ versus the Al^{3+} garnets, the average energy of the 5d manifold is ∼1000 cm^{-1} *higher*. While this calculation of the centroid shift can only be an estimate without accurate measurement of the deeper UV excitation bands, it does not appear that a larger 5d centroid shift leads to the redder Ce^{3+} emission in the silicate garnets. This is not unreasonable given that the Ce^{3+} 5d centroid shift is somewhat smaller when comparing silicates versus aluminates.[10,35] Therefore, we believe that a larger crystal field splitting causes the red shift in these silicate phosphors when compared to YAG.

The splitting of the 5d manifold in garnets can be correlated to a $T_{2g}-E_g$ cubic splitting with an additional splitting due to the distortion of cubic coordination into a dodecahedron.[32,37,38] Consequently, the effect of the crystal field splitting on the position of the lowest 5d level can be separated into two major components: the splitting between the T_{2g} and E_g levels (signified by the 10 Dq phenomenological parameter) and the splitting of the E_g levels. While the barycenter of the E_g levels can be derived from experimental measurements (Figure 6b), we have not observed any excitation/absorption bands that can be clearly assigned to T_{2g} levels. However, the barycenter of the T_{2g} levels can be estimated by taking into account that in cubic and distorted cubic coordinations, the energy difference between the E_g barycenter and the 5d centroid is 1.5 times larger than the energy difference between the T_{2g} barycenter

(34) van der Kolk, E.; Dorenbos, P.; van Eijk, C. W. E.; Basun, S. A.; Imbusch, G. F.; Yen, W. M. *Phys. Rev. B* **2005**, *71*, 165120.
(35) Dorenbos, P. *Phys. Rev. B* **2002**, *65*, 235110.
(36) Dorenbos, P. *J. Lumin.* **2003**, *105*, 117.
(37) Randic, M. *J. Chem. Phys.* **1962**, *36*, 2094.
(38) Burdett, J. K.; Hoffmann, R.; Fay, R. C. *Inorg. Chem.* **1978**, *17*, 2553.

Table 4. Ce^{3+} 5d Centroid and T_{2g}/E_g Barycenters for Various Eight-Coordinated Hosts

host	T_{2g} barycenter (cm^{-1})	E_g barycenter (cm^{-1})	5d centroid (ϵ_c) (cm^{-1})	$(\epsilon_c-E_g)/(T_{2g}-\epsilon_c)$	ref
CaF_2	53 400	32 300	44 940	1.49	40
$LiYF_4$	50 700	37 300	45 340	1.50	40
YPO_4	44 800	35 400	41 040	1.50	40
$Y_3Al_5O_{12}$	43 900	25 650	36 600	1.50	41

and the 5d centroid.[39] This relationship can be seen for the Ce^{3+} 5d levels in other hosts with cubic or dodecahedral coordination[40,41] (Table 4). Taking into account the estimated centroid shift of 13 300 cm^{-1} and this relationship, 10 Dq is then estimated for these new garnets (Table 3). The values of 10 Dq for the silicate and aluminate garnets are not significantly different, especially considering the accuracy of the estimation. Therefore, it is apparent that the splitting between the lowest two Ce^{3+} 5d levels is the most significant difference between the silicate and aluminate garnets that leads to a lower energy emission band (Table 3).

As discussed above, the lowest two 5d levels for Ce^{3+} in YAG can be correlated to E_g levels in cubic coordination. In dodecahedral coordination, the lowest absorption band corresponds to transitions to a $d_{x^2-y^2}$ orbital with transitions to the d_{z^2} orbital making up the next absorption/excitation band.[37,38] The differences between the splitting of the Ce^{3+} E_g levels in the Si^{4+} and Al^{3+} garnets could then be due to changes in the shape of the dodecahedral coordination polyhedra in these garnets since the coordination shape plays a critical role in the crystal field splitting of the 5d manifold.[10,35] For example, one difference between typical Al^{3+} garnets and this new Si^{4+} garnet are the O−{C}−O bond angles for the dodecahedral−tetrahedral shared edge as described in section 3.1. This change in the shape of the coordination polyhedra around Ce^{3+} could change the crystal field splitting and shift the lowest 5d level to lower energy.

In this argument above, we have not addressed the changes in the position of the lowest 5d level that also could arise through Lu^{3+}/Ca^{2+} disorder. One possible effect from Lu^{3+}/Ca^{2+} disorder is that the crystal field splitting is modified due to changes in the anion polarization.[42] The larger and lower charged Ca^{2+} ions cannot polarize the O^{2-} charge density as well, leading to a stronger crystal field on Ce^{3+} in these silicate garnets. Taking into account the anion polarizability can also lead to an assignment for the different "sites" observed in this material since the O^{2-} polarization toward Ce^{3+} in these garnets should also vary due to Lu^{3+}/Ca^{2+} disorder. The smaller and highly charged Lu^{3+} ions should polarize O^{2-} charge density away from Ce^{3+}, thereby reducing the crystal field on Ce^{3+}, leading to an assignment of the high-energy sites to Ce^{3+} ions that are in Lu^{3+} rich regions. Correspondingly, we can assign the low-energy sites to Ce^{3+} ions that are in Ca^{2+} rich regions. Alternatively, the local coordination around Ce^{3+} could change depending on

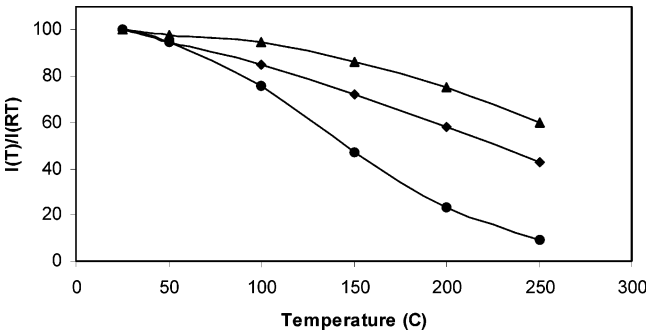

Figure 8. Luminescence intensity (λ_{ex} = 470 nm) versus temperature for YAG:Ce (triangles), $(Lu_{0.94}Ce_{0.06})_2CaMg_2Si_3O_{12}$ (diamonds) and a redder (Tb,Gd)AG:Ce phosphor with $\lambda_{max} \sim 580$ nm (circles). The thermal quenching of the luminescence of the new phosphor is greater than YAG but significantly less when compared to redder modifications of Al^{3+} garnets.

presence of Lu^{3+} or Ca^{2+} in the nearest neighbor dodecahedral site. Therefore, we caution that this analysis of the Ce^{3+} luminescence is vastly simplified. Further work will be necessary to determine the fundamental relationship of the Ce^{3+} 5d levels with the structure and composition of garnet based hosts.

As noted in the Introduction, the observation of red emission is not enough for practical phosphor implementation without high quantum efficiencies at room and elevated temperatures. The quantum efficiency of $Lu_2CaMg_2Si_3O_{12}$:Ce^{3+} under 470 nm excitation is comparable to typical garnet phosphors. The thermal quenching of our new phosphor is somewhat stronger in comparison to YAG:Ce but is significantly better than Al^{3+} garnet compositions that are modified for red emission (Figure 8). Given the relatively small Stokes shift for the lower energy Ce^{3+} site in the silicate garnet, it is unlikely that level crossing between the lowest 5d level and the 4f states is the cause of the thermal quenching. As noted above, photoionization may also play a critical role for the efficient of Ce^{3+} luminescence.[23] Some insight toward photoionization quenching can be gained by analyzing the Ce^{3+} quantum efficiency in these new garnets with Ge^{4+} substitution. While garnet phase formation is enhanced with Ge^{4+} addition (Figure 3), the Ce^{3+} quantum efficiency is reduced at higher Ge^{4+} concentrations with stronger thermal quenching (Table 1). At higher Ge^{4+} concentrations, the position of the lowest 5d level of Ce^{3+} is at higher energy, while the host lattice band gap will be lowered. Assuming that the position of the Ce^{3+} ground state does not change with respect to the host lattice valence band, this will reduce the energy barrier for photoionization, decreasing both the room temperature and high-temperature quantum efficiency. Similar trends for Ce^{3+} luminescence at room and elevated temperatures have been observed in the YAG−YGG system,[2,7−9] where there has been extensive work in placing RE^{3+} ground states in the band gap of these hosts,[43,44] making photoionization estimates more quantitative. The variation in room- and high-temperature efficiency with Ge^{4+} concentration leads us to conclude that quenching is likely occurring via photoionization. However, unequivocal as-

(39) Cotton, F. A. *Chemical Applications of Group Theory*; Wiley-Interscience: New York, 1990.
(40) van Pieterson, L.; Reid, M. F.; Wegh, R. T.; Soverna, S.; Meijerink, A. *Phys. Rev. B* **2002**, *65*, 045113.
(41) Tomiki, T.; Kohatsu, T.; Shimabukuro, H.; Ganaha, Y. *J. Phys. Soc. Jpn.* **1992**, *61*, 2382.
(42) Aull, B. F.; Jenssen, H. P. *Phys. Rev. B* **1986**, *34*, 6640.
(43) Thiel, C. W.; Cruguel, H.; Wu, H.; Sun, Y.; Lapeyre, G. J.; Cone, R. L.; Equall, R. W.; Macfarlane, R. M. *Phys. Rev. B* **2001**, *64*, 085107.
(44) Thiel, C. W.; Cruguel, H.; Sun, Y.; Lapeyre, G. J.; Macfarlane, R. M.; Equall, R. W.; Cone, R. L. *J. Lumin.* **2001**, *94*−*95*, 1.

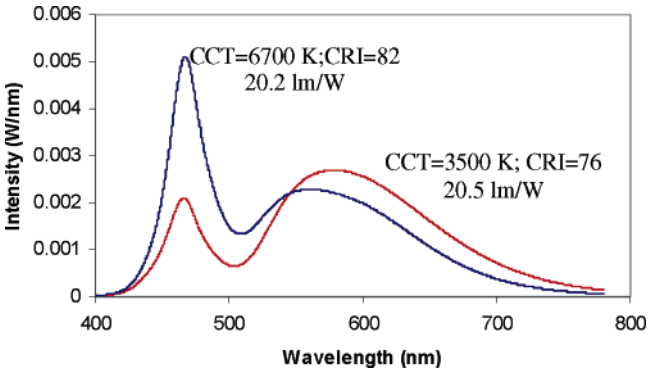

Figure 9. Spectra of LED based lamps with high CCTs that use solely typical Ce^{3+} garnets and low CCTs using blends of typical Ce^{3+} garnets with $(Lu_{0.94}Ce_{0.06})_2CaMg_2Si_3O_{12}$.

signment of the quenching mechanism of the silicate garnets requires further experimental evaluation. In addition, optimized sample synthesis could also lead to improvements in the overall phosphor efficiency. In a practical sense, however, phosphor selection in this system will be straightforward since the $Lu_2CaMg_2Si_3O_{12}:Ce^{3+}$ composition is significantly redder (as desired for lower CCT and higher CRI light sources) and has a higher quantum efficiency.

3.3. Performance in LED Lamps. The inherent disorder in $\{Lu_2Ca\}[Mg]_2(Si)_3O_{12}$ and subsequent energy transfer between high- and low-energy Ce^{3+} ions leads to an advantage in the practical use of these phosphors. There appears to be minimal absorption for $\lambda > 525$ nm for these $Lu_2CaMg_2Si_3O_{12}:Ce^{3+}$ phosphors (Figure 4a). Comparing the relative position of the high-energy and low-energy Ce^{3+} sites (Figure 5) and the excitation/reflectance spectra of samples with 4.5% Ce^{3+} (nominal) (Figure 4), it appears that a majority of the Ce^{3+} ions are in high-energy sites, while the emission spectra has significant red emission characteristic of the low-energy Ce^{3+} sites. The sensitization of the low-energy Ce^{3+} sites by the high-energy Ce^{3+} sites enables red emission from these sites, without a high concentration of low-energy Ce^{3+} sites that have absorption strength in the green spectral region (Figure 5b). This reduces phosphor reabsorption losses in these materials.

The high quantum efficiency for these $Lu_2CaMg_2Si_3O_{12}:Ce^{3+}$ phosphors combined with minimal reabsorption effects should lead to good performance in LED based lamps. The lumen output of the lower CCT blend using $Lu_2CaMg_2(Si,Ge)_3O_{12}:Ce^{3+}$ was 85−100% of higher CCT lamps using only typical Ce^{3+}-doped garnets, depending on the phosphor color point for the high CCT lamps (Figure 9). Further analysis of these devices for photons emitted vs photons absorbed gives a ∼97% conversion efficiency of the low CCT phosphor blend compared to the high CCT phosphor, in reasonable agreement with our plaque quantum efficiency measurements. Further improvements in the phosphor conversion efficiency are possible given optimization in the phosphor coatings as well as by incremental improvements in the phosphor quantum efficiency and absorption by synthesis optimization.

4. Conclusions

In this report, we have detailed the synthesis and luminescence properties of new silicate/germanate garnet phosphors, $Lu_2CaMg_2(Si,Ge)_3O_{12}:Ce^{3+}$, that can meet many of the red phosphor requirements for general illumination LED lighting. The composition regions for phase stability have been described and explained using known crystal chemistry trends within the garnet family of materials. In addition, we have presented an initial explanation for the significant red shift in the emission band of Ce^{3+} in this garnet when compared to YAG:Ce^{3+}, the high quantum efficiency of this material, and the reduced absorption of this phosphor in the yellow-green spectral region. There are open questions regarding the crystal chemistry and luminescent properties of these materials, primarily the exact composition and site occupation in these materials and their overall efficiency. Answering these questions will require further investigation and fundamental analysis. However, at this time, the conversion efficiency of low CCT blends that use these new phosphors can be almost equivalent to commercial Ce^{3+}-doped garnets in certain LED packages.

Acknowledgment. The authors thank E. A. Bachniak, H. A. Comanzo, M. C. Hill, H. C. Peters, and C. Henderson for sample synthesis and initial luminescence measurements and S. E. Weaver for the fabrication of LED lamps. This work was primarily supported by GELcore with partial support of the spectroscopic measurements by the U.S. Department of Energy through Contract No. DE-FC26-04NT41945. However, any opinion, findings, conclusions or recommendations expressed herein are those of the authors and do not necessarily reflect the views of the Department of Energy.

CM060898C